ACS OMEGA

http://pubs.acs.org/journal/acsodf

Article

First-Principles Study of 3d Transition-Metal-Atom Adsorption onto Graphene Embedded with the Extended Line Defect

Zhaoyong Guan,* Shuang Ni, and Shuanglin Hu

Cite This: *ACS Omega* 2020, 5, 5900−5910

Read Online

ACCESS | Metrics & More | Article Recommendations | Supporting Information

ABSTRACT: A type of line defect (LD) composed of alternate squares and octagons (4−8) as the basic unit is currently an experimentally available topological defect in the graphene lattice, which brings some interesting modifications to the magnetic and electronic properties of graphene. The transitional-metal (TM) atoms adsorb on graphene with a line defect (4−8), and they show interesting and attractive structural, magnetic, and electronic properties. For different TMs such as Fe, Co, Mn, Ni, and V, the complex systems show different magnetic and electronic properties. The TM atoms can spontaneously adsorb at quadrangular sites, forming a metallic atomic chain along LD on graphene. The most stable configuration is the hollow site of a regular tangle. The TMs (TM = Co, Fe, Mn, Ni, V) tend to form extended metal lines, showing a ferromagnetic (FM) ground state. For the Co, Fe, and V atoms, the system is half-metal. The spin-α electron is insulating, while the spin-β electron is conductive. For the Mn and Ni atoms, Mn-LD and Ni-LD present a spin-polarized metal; for the Fe atom, Fe-LD shows a semimetal with Dirac cones. For Fe and V atoms, both Fe-LD and V-LD show spin-polarized half-metallic properties. And its spin-α electron is conducting, while the spin-β electron is insulating. Different TMs adsorbing on a graphene nanoribbon forming the same stable configurations of metal lines show different electronic properties. The adsorption of TMs induces magnetism and spin polarization. These metal lines have potential applications in spintronic devices and work as a quasi-one-dimensional metallic wire, which may form building blocks for atomic-scale electrons with well-controlled contacts at the atomic level.

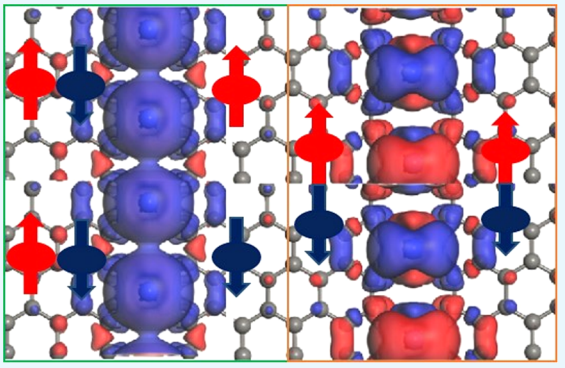

1. INTRODUCTION

In 2004, Geim et al. successfully isolated graphene using the micromechanical method.[1] Graphene is a 0 eV gap semimetal,[2] with Dirac cone[3−5] and a very high carrier mobility.[6−8] A theoretical study indicated that a half-metallic electronic structure could be realized in a zigzag-edged graphene nanoribbon driven by a transverse electric field.[9,10] Motivated by changing chemical potentials,[11−13] edge functions,[14,15] chemical doping with boron and nitrogen atoms,[11,13,16] domains,[17,18] van der Waals structures,[19−21] topological line defect (LD),[14,22−24] and other methods[25−27] are used to tune the magnetic and electronic properties of low-dimensional materials. As a result, a completely spin-polarized electronic transport is expected in these nanostructures.[11−14] Limited by a strong E-field[9,10] and the operating accuracy of chemical functions,[15,28−30] it is hard to realize experiments.[9,11] As a result, spin polarization of a graphene nanoribbon has not yet been observed in experiments.[14]

Another method of realizing spin polarization and half-metallicity is doping with a transitional metal (TM),[16,31−36] such as cobalt (Co),[37−40] iron (Fe),[41−43] manganese (Mn),[35,44,45] nickel (Ni),[46−48] and vanadium (V).[49] A single TM atom adsorbing on either perfect[50] or defective graphene[32,36] has been widely investigated,[36,51,52] showing quite attractive geometrical, magnetic, and electronic properties.[36,49,52−54] Atomic chain adsorption on the surface is also observed in the experiments.[31,55] But there are only few theoretical studies that investigate atomic chains, especially metal atomic chains, on defective graphene and graphene ribbons.[33] It is the objective of the present work to study the adsorption of TM chains on graphene and systematically investigate the geometrical, magnetic, and electronic properties.

In 2018, Zhong et al. successfully synthesized periodically embedded four- and eight-membered rings with the on-surface method.[56] And graphenes with LD are semiconductors with a reduced band gap.[56,57] In our previous investigation, the electronic and mechanical properties of graphene with LD consisting of squares and octagons have been predicted.[57] The LD could introduce defective states in the original forbidden

Received: December 5, 2019
Accepted: March 4, 2020
Published: March 16, 2020

https://dx.doi.org/10.1021/acsomega.9b04154
ACS Omega 2020, 5, 5900−5910

band gap.[14,57] And the valance band maximum (VBM) and the conduction band minimum (CBM), which are usually relative to the chemical active sites, are also transferred from the edge sites to the LD atoms.[57−59] When the TM atoms adsorb on graphene, they intend to adsorb at these defective sites with high chemical active properties of the graphene.[31−33,58,60] Salmeron found that water could split graphene and intercalates.[61] Cheng investigated single TM atom adsorption on graphene.[50−52] Researchers have only recently focused on the single TM atom adsorption on graphene sheet in their work, but the topological, structural, magnetic, and electronic properties of the TM atom adsorption on graphene are still unknown. Therefore, it is urgent to investigate how the TM atom adsorbs on graphene with LD, which consists of octagons and squares. Besides, both the VBM and CBM of graphene embedded with LD, consisting of octagon and pentagon (5−8−5)[14,57] or square and octagon (4−8),[57] localize at the LD sites. The effects of the adsorption of TM on graphene are still unknown. Furthermore, the well-defined atomic structure of nanowire can help overcome practically one of the challenges of nanoelectronics.[62] This point is urgently needed for the development of molecular electronics,[63−66] single-molecule sensors,[67−69] and electrocatalytic energy conversion.[70]

2. COMPUTATIONAL DETAILS

The calculations of defective graphene nanoribbon, adsorption with TMs are performed by using a numerical radial function basis set DMol^3 package,[71,72] which is based on the density functional theory. The Perdew−Burke−Ernzerhof (PBE)[73] functional is used to describe the exchange−correlation interaction between electrons. The double numerical atomic orbital augmented by polarization functions (DNP)[74] is adopted as the basis set. The vacuum space along the z-direction is set as large as 16 Å to avoid the interaction between imaginary images. The real-space global cutoff radius is set to 5.6 Å. Geometry optimization, total energy, density of states (DOS), and band structure calculations are sampled with $8 \times 3 \times 1$, $16 \times 6 \times 1$, $20 \times 8 \times 1$, and 160 Monkhorst−Pack k-point[75] meshes, respectively. For TM (TM = Co, Fe, Mn, Ni, V) adsorption on LD-embedded graphene sheet, a large $4 \times 1 \times 1$ (5 carbon hexagons along the $\vec{b}$ direction) supercell is adopted to simulate isolated TM adsorption, while a smaller $2 \times 1 \times 1$ (11 hexagons along $\vec{b}$ direction) supercell is used to calculate the adsorption of "metal chains" on the graphene sheets. The energy and electron density is converged to 1×10^{-6} au (1 Hartree = 27.21 eV). Geometry optimizations are performed until the corresponding values are less than 2×10^{-3} au/Å on the gradient, 5×10^{-3} Å on the displacement, and 1×10^{-6} au on the total energy. Graphene is used as a testing system to check accuracy. The C−C bond length in graphene is calculated to be 1.42 Å, which is consistent with the experimental value.[6] To analyze the interaction strength between TM and graphene, charge partitioning is calculated by the Hirshfeld method.[76]

3. RESULTS AND DISCUSSION

3.1. Geometry of Graphene with LD. We first optimize the geometry of graphene with LD, which consists of successive squares and octagons. The corresponding optimized geometry is shown in Figure 1. The corresponding C−C bond lengths of octagon are 1.50, 1.39, and 1.43 Å. While for the square, the corresponding C−C bond lengths are 1.50 and 1.40 Å.[57] Compared to perfect graphene, whose C−C bond length is 1.42 Å, some C−C bonds are slightly compressed (1.40 and 1.39 Å), while others are enlarged (1.50 Å). More details can be found in Figure S1. And this is consistent with the previous simulated results.[56] Six adsorption sites have been investigated. H stands for the hollow site, and H_1, H_2, and H_3 denote perfect hollow sites of perfect hexagon, octagon, and square, respectively. B_1 and B_2 denote the bridge site of perfect hexagonal and defective rings, respectively. T_1 indicates the top site of perfect hexagons.

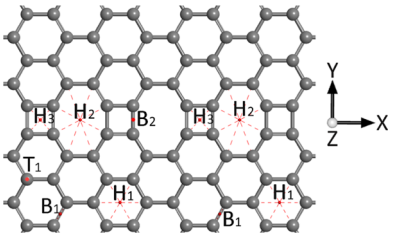

Figure 1. Extended LD made of paired tetragonal and octagonal rings in graphene nanoribbon. H_1, H_2, H_3, T_1, B_1, and B_2 denote adsorption sites, hollow, top and bridge sites, respectively. The gray ball presents the carbon atom.

In this work, the adsorption energy (E_{ad}) is defined as

$$E_{ad} = E_{mg} - E_{TM} - E_g$$

E_{ad} denotes the adsorption energy of TM, E_{mg} denotes the energy of the complex of TM and graphene, and E_{TM} and E_g represent the energies of the single TM atom and graphene with LD, respectively. E_{TM} is calculated using stable bulk energy of TM divided by the number of the atoms.[77] As more transition-metal atoms adsorb on the graphene with grain boundary, the transition-metal atoms form clusters at the grain boundary areas. To simply the problem, we here mainly investigate the adsorption of low-concentration TM atoms on graphene.

3.2. Electronic Structure and Magnetic Properties of TM (TM = Co, Fe, Mn, Ni, V) Adsorption on Graphene. In this section, the geometry of single TM atom on graphene is investigated. The adsorption configurations of H_1, H_2, H_3, B_1, B_2, T_1, and T_2 sites are calculated. The corresponding supercell sizes along the lattices $\vec{a}$ and $\vec{b}$ are 17.30 and 13.71 Å, respectively. The distance between the metal atom and the corresponding image is at least 12 Å to avoid the artificial interaction between metal atom and its image.

3.2.1. Electronic Structure and Magnetic Properties of Co Atom Adsorption on Graphene. The calculated E_{ad}, the corresponding bond length between carbon and metal atoms, charge transfer, magnetic moment (MM) of system, and TM atom are shown in Table 1. The different adsorption sites H_1, H_2, H_3, and B_1 correspond to different E_{ad} values. Compared to H_1 and H_2 configurations, the hollow site of square (H_3) has the highest stability. And the corresponding E_{ad} value is 1.91 eV, which is larger than H_1 (1.41 eV), H_2 (1.12 eV),[49] and B_1 (1.04 eV). For the H_3 site, the corresponding Co−C bond length is 2.00 Å, implying that the Co atom prefers to stay in the center of square. The B_1 site has the smallest E_{ad} value (1.04 eV), which means that this site is the most unstable in energy. For H_2 and H_1 sites, the Co atom stays in the center of the octagon and hexagon, respectively. And the E_{ad} value of H_2 is slightly smaller than that of the H_3 site, but larger than that of the B_1 site. It seems that the Co atom tends to stay at the

https://dx.doi.org/10.1021/acsomega.9b04154
ACS Omega 2020, 5, 5900−5910

Table 1. Adsorption Energies and Structural Properties for H_1, H_2, H_3, and B_1 Sites Investigated in This Work[a]

			distance (Å)						
Co sites	E_{tot} (eV)	E_b (eV)	d_1	d_2	d_3	d_4	$\Delta\rho$ (e)	MM (μ_B)	MM_{Co} (μ_B)
H_2	−686.01	1.12	2.19	2.19	2.18	2.18	0.29	1.63	0.99
H_3	−686.80	1.91	2.00	2.00	2.00	2.00	0.29	1.14	0.99
H_1	−686.30	1.41	2.15	2.14	2.14	2.15	0.28	1.36	1.47
B_1	−685.93	1.04	2.12	2.13			0.19	2.54	2.50

[a]The properties listed are E_{ad} (eV); bond lengths d_1, d_2, d_3, and d_4 (Å); charge transfer between TM and graphene $\Delta\rho$ (e); and total magnetic moments MM (μ_B) and TM MM_{Co} (μ_B).

hollow site of square, octagon, and hexagon. And for the hollow site, 0.30 e electron transfers from the Co atom to graphene. For the bridge site, charge transfer is only 0.19 e electron, which implies weaker interaction between the Co atom and graphene. E_{ad}, charge transfer, and magnetic properties are also investigated. For H_2, H_3, and H_1, the total magnetic moment (MM) is 1.63, 1.14, and 1.36 μ_B, respectively. While for B_1, the total MM is 2.54 μ_B. Most of magnetic moments come from the Co atom, which is confirmed by the spin densities of H_2, H_3, H_1, and B_1, as shown in Figure 3. For the H_1 configuration, the Co atom contributes 1.72 μ_B (total MM is 1.47 μ_B). Each next-nearest carbon atom contributes 0.03 μ_B MM.

For the H_2 configuration, the Co atom contributes 0.99 μ_B MM. For the H_3 configuration, the Co atom contributes 1.47 μ_B MM.[50,52] For the B_1 configuration, the Co atom contributes 2.50 μ_B MM. From Figure 2, it can be concluded that the magnetic moment mainly localizes at the Co atom and quickly decreases at a long distance from the Co atom.[50,52]

In the above section, it is found that the H_2 site is the most stable adsorption site. When the two Co atoms adsorb on graphene, they intend to form a "metallic line".[78] The corresponding bond length of Co−C is 2.01 Å, and the distance between the Co atoms is about 4.30 Å, which is larger than corresponding bond length of the Co−Co atom (2.51 Å) in the bulk. Two Co atoms can ferromagnetically or antiferromagnetically couple with each other, and the corresponding FM and antiferromagnetic (AFM) spin densities are shown in Figure 3a,b, respectively, where blue and red represent spin-α and spin-β densities of electrons, respectively. In Figure 3a, both Co atoms show spin-α density (they have the same color) and hence they ferromagnetically couple with other. Each Co atom has 1.01 μ_B MM, and Co-LD has 2.00 μ_B MM. While two Co atoms show different spin-α and spin-β densities, as shown in Figure 3b, which implies that the two Co atoms antiferromagnetically couple with other. One Co atom has −1.00 μ_B MM, while the other has 1.00 μ_B MM, so that the total MM equals 0.00 μ_B. The MM value decreases quickly when it is far away from the Co atom. Carbon atoms far away from LD have no magnetic moment.[54] Compared to the original graphene with LD, the Co atoms indeed introduce magnetism and spin polarization.[14,51,52,54,57] The energy difference (ΔE) is defined as the energy difference

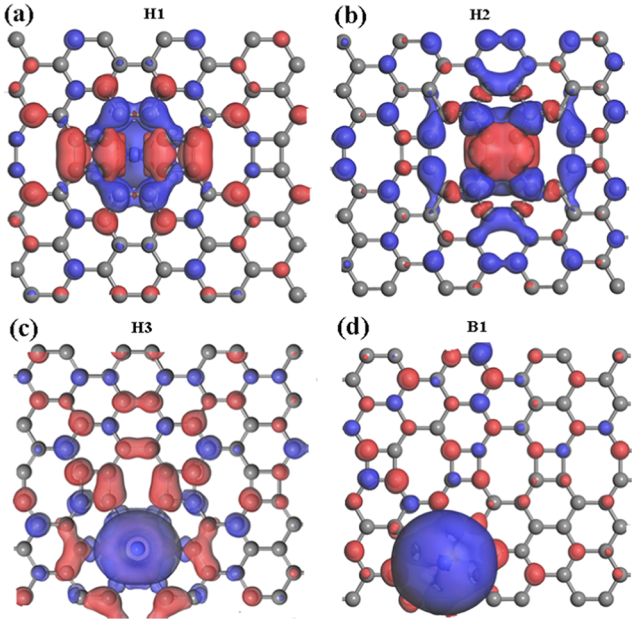

Figure 2. Spin density of the Co atom adsorbing on graphene with different positions. Adsorption sites of the (a) hollow site of the octagon (H_2), (b) hollow site of the quadrangle (H_3), (c) hollow site of perfect hexagon (H_1), and (d) the bridge site (B_2) of the hexagon. The isovalue is 0.003 e/Å^3.

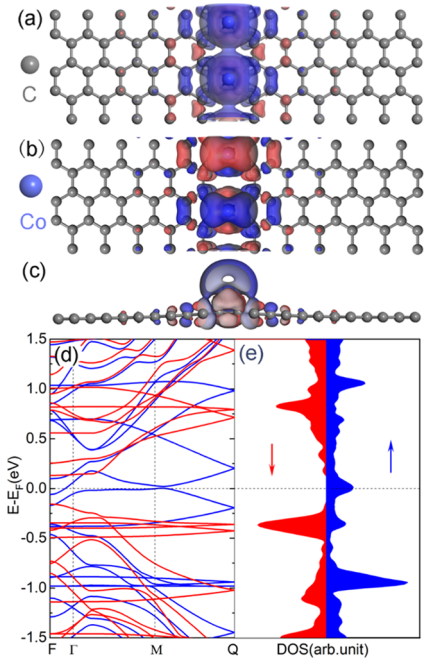

Figure 3. (a−d) Spin density, spin-polarized band structure, and partial DOS (PDOS) of Co-LD. (a) Spin density of (c) FM and (b) antiferromagnetic (AFM) configuration of Co-LD. The gray and violet balls represent C and Co atoms, respectively. (d) Band structure and (e) DOS of Co-LD. The blue and red lines represent spin-α and spin-β electrons, respectively. Here, the isovalue is set 0.003 e/Å^3. The gray and blue balls represent carbon and cobalt atoms, respectively.

https://dx.doi.org/10.1021/acsomega.9b04154
ACS Omega 2020, 5, 5900−5910

Table 2. Adsorption Energies and Structural Properties of H_1, H_2, H_3, and B_1 Sites Investigated in This Work[a]

			distance (Å)						
Fe site	E_{tot} (eV)	E_{ad} (eV)	d_1	d_2	d_3	d_4	$\Delta\rho$ (e)	MM (μ_B)	MM_{Fe} (μ_B)
H_2	−685.49	0.90	2.32	2.32	2.72	2.72	0.26	4.02	3.54
H_3	−686.06	1.42	2.05	2.05	2.05	2.05	0.35	2.02	2.45
H_1	−685.63	1.04	2.12	2.12	2.12	2.12	0.28	2.29	2.17
B_1	−684.99	0.03	2.35	2.35			0.17	4.36	4.17

[a]The properties listed are E_{ad} (eV); bond lengths d_1, d_2, d_3, and d_4 (Å); charge transfer between the Fe atom and graphene $\Delta\rho$ (e); and total magnetic moments MM (μ_B) and TM (irion) MM_{Fe} (μ_B).

between FM and AFM magnetic configurations, defined as follows

$$\Delta E = E_{FM} - E_{AFM}$$

where E_{FM} and E_{AFM} stand for energies of FM and AFM states, respectively. For Co adsorbing on graphene with LD, the corresponding ΔE value is 0.10 eV, which implies the FM ground state. ΔE is the energy difference between the AFM and FM phases per unit cell. Here, ΔE can be approximately chosen to be the total energy difference between the AFM and FM phases.

The corresponding band structure and DOS are shown in Figure 3c,d, respectively. From the band structure, we can find that the FM ground state is spin-polarized. The spin-α electrons show half-metallic properties, while spin-β electrons show semiconductive properties with a band gap of 0.30 eV. And this is consistent with the analysis of PDOS, shown in Figures 3d and S2. The states near the Fermi level are mainly contributed by Co atoms and partially by the carbon atoms (octagon and square), shown in Figure S2. The gap of spin-β electron is 0.30 eV, much larger than the excited energy of electron at room temperature (300 K, 0.026 eV). Therefore, the gap is large enough to ensure the stability of half-metallicity. The Co atoms tend to form a metallic line, which could work as a spin filter. When the spin-α and spin-β electrons come across LD adsorption with Co atoms, only spin-α electrons could pass through the graphene nanoribbon, while the spin-β electrons are unable to pass.

3.2.2. Electronic Structure and Magnetic Properties of Fe Atom Adsorption on Graphene. In this section, we investigate the structural, magnetic, and electronic properties of Fe-LD. First, single Fe atom adsorption on graphene is studied and shown in Table 2, from which 2it can be found that the most stable adsorption site is H_3. The corresponding E_{ad} value is about 1.42 eV, with the corresponding Fe−C bond length of 2.05 Å, meaning the Fe atom is in the center of the square. While for H_2, H_1, and B_1 sites, the corresponding E_{ad} values are 0.90, 1.04, and 0.03 eV. For the H_1 configuration, E_{ad} is similar to that of Fe atom adsorption on perfect graphene, 1.02 eV.[50,52] The Fe−C bond lengths of the H_3 site are 2.32 and 2.72 Å, respectively, which are larger than the 2.08 Å.[51] The E_{ad} value of the most stable H_3 site is 0.40 V larger than that of the H_1 site. The H_2 site (hollow site of octagon) is 0.10 eV lower than the H_1 site in energy. While B_1 site is the most unstable site in the considered four sites, it only has 0.03 eV, which means that the Fe atom adsorption at this site is easily shifted for the smaller migration barrier.[49] And the corresponding Fe−C bond length is 2.35 Å, which is larger than that of the H_1 site (2.12 Å).

When the TM atom adsorbs on graphene, it usually follows charge transfer. For the H_2 site, the Fe atom loses 0.35 e electron. While for the H_2 and H_1 sites, the corresponding charge transfers are 0.26 and 0.28 e electrons. For the most unstable B_1 site, it is only 0.17 e electron, which means that charge transfer between the Fe atom and graphene could be neglected. The charge transfer and E_{ad} show the same trend. Only one part of electrons transfer from the Fe atom to graphene. For the H_3 site, it has 2.00 μ_B, and the Fe atom contributes 2.45 μ_B MM, whose spin density is shown in Figure 4c. Each carbon atom of the square has −0.03 μ_B MM. For

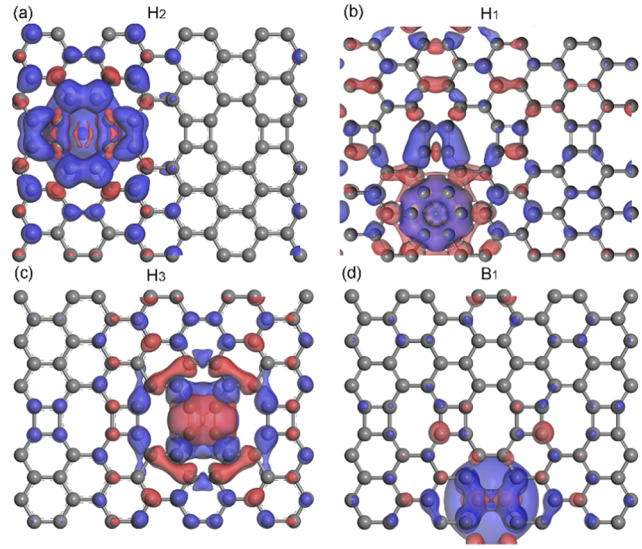

Figure 4. Spin density of iron adsorption on the graphene nanoribbon. Single iron atom adsorption on (a) H_2, (b) H_1, (c) H_3, and (d) B_1 sites. The isovalue is set to 0.003 e/Å^3. Blue and red present spin-α and spin-β electrons, respectively.

carbon atoms far away from LD, there is no magnetic moment distribution. For the H_2 site, the whole system has 4.02 μ_B MM, while the Fe atom contributes 3.54 μ_B MM. Each carbon atom of the octagon contributes 0.02 and 0.04 μ_B MM. For the H_1 site, the Fe atom has 2.29 μ_B MM, and the whole system has 2.17 μ_B MM. Each hexagonal carbon atom has −0.02 μ_B MM, as shown in Figure 4b. For the B_1 site, the Fe atom has 2.17 μ_B MM, and the whole system has 4.36 μ_B MM. Each carbon atom connected to the Fe atom has 0.02 μ_B MM, as shown in Figure 4d. In a word, it can be found that the magnetic moment mainly localizes at the Fe and nearby C atoms.[52]

In this part, the magnetic and electronic properties are systematically investigated, and spin density, spin-polarized band structure, and DOS of Fe-LD are shown in Figure 5. The Fe atom prefers to stay at the H_3 site, so two Fe atoms tend to form a "metal line".[33] The corresponding Fe−C bond length is 2.07 Å (2.07 Å × 4), which is consistent with the H_3 site, as shown in Figure 4c, and the corresponding Fe atom has 2.40

https://dx.doi.org/10.1021/acsomega.9b04154
ACS Omega 2020, 5, 5900−5910

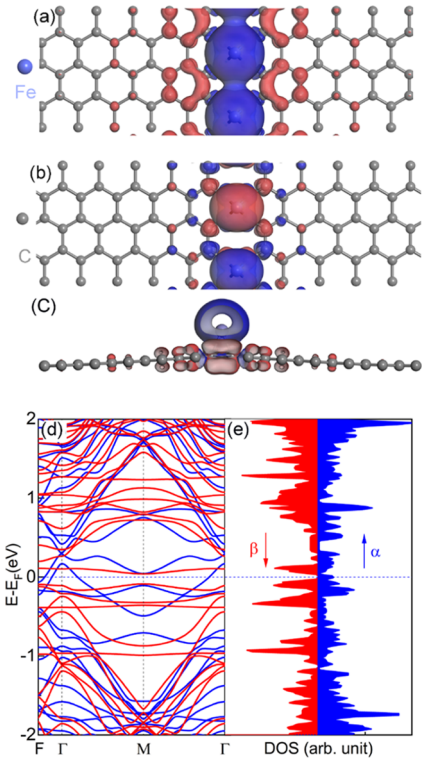

Figure 5. (a–d) Spin density, spin-polarized band structure, and PDOS of Fe-LD. (a) Spin density of (c) FM and (b) AFM Fe-LD. The blue and gray balls denote Fe and carbon atom, respectively. (d) Band structure and (e) PDOS of Fe-LD. The blue and red lines represent spin-α and β electrons, respectively. Here, the isovalue is 0.003 e/Å^3. The blue and gray balls represent iron and carbon atoms, respectively.

μ_B MM. The other Fe−C bond length is 2.12 Å, which is consistent with that of the H_1 site, and the Fe atom has 2.40 μ_B MM. Two Fe atoms lose about 0.38 e electron, and each Fe atom loses 0.19 e electron, respectively. Two Fe atoms have the same spin, so Fe atoms ferromagnetically couple with each other, as shown in Figure 5a. The carbon atoms of square have opposite spins of −0.04 and −0.05 μ_B MM, respectively. The AFM configuration is shown in Figure 5b. And one Fe atom has 2.40 μ_B MM, while the other has −2.40 μ_B MM. One carbon atom bounded with the Fe atom (2.40 μ_B) has 0.04 μ_B, and other carbon atoms has −0.04 μ_B. The ΔE value defined as the energy difference between FM and AFM configuration is about 0.05 eV. The spin-polarized band structure and DOS of the FM ground states are also calculated, as shown in Figure 5c,d. There is a Dirac cone for spin-α electron above the Fermi level. It implies that Fe-LD keeps the original Dirac cone of the perfect graphene, but it reduces the original generacy.[6] Besides, the states near the Fermi level are mainly contributed by the spin-α electrons, while the contribution from spin-β electrons could be eliminated. The spin-α electron is conductive, while the spin-β electron is an insulator with a band gap of 0.13 eV, which implies that Fe-LD is half-metal. The gap of the spin-β electron could ensure that the electron could not be thermally excited from the VBM to CBM at room temperature. The PDOS of Fe-LD is also calculated, and the result is shown in Figure S3. From PDOS, we can find that the states near the Fermi level are mainly contributed by Fe atoms. It implies that bonding states are contributed by Fe atoms. The first peak above the Fermi level also comes from the contribution of Fe atoms, which implies that antibond states are composed of spin-β electrons.

3.2.3. Electronic Structure and Magnetic Properties of Mn Atom Adsorption on Graphene. The structural, magnetic, and electronic properties of single Mn atom adsorption on graphene with LD are also systematically investigated. And all results are shown in Table 3. For the H_2 site, the Mn atom lies in the center of the hexagon, and the corresponding Mn−C bond length is 2.44 Å. The E_{ad} value is 1.16 eV. The Mn atom loses 0.31 e electron. For the H_3 site, the Mn−C bond length is 2.30 Å and the Mn atom lies in the center of the square.

The corresponding E_{ad} value is 1.39 eV, which is the largest value among the considered sites. For the H_1 site, the corresponding Mn−C bond length is 2.63 Å and E_{ad} = 0.92 eV, which is consistent with the previous result.[51] For the B_1 site, the corresponding Mn−C bond length is 2.40 Å and E_{ad} is quite small. The $\Delta\rho$ value between Mn and graphene is only 0.26 e electron, which is smaller than other configurations.

In the above section, the structural properties of Mn adsorption on graphene are investigated. In this section, the magnetic properties of all kinds of configurations are also listed. For the H_2 site, the Mn atom contributes 5.23 μ_B MM, while Mn-LD has 5.05 μ_B MM. For the H_3 configuration, the Mn atom contributes 5.04 μ_B MM, while the whole system has 5.06 μ_B MM. For the H_1 configuration, the Mn atom lies in the center of the hexagon. And the Mn atom has 5.47 μ_B MM, while the whole system has 5.79 μ_B MM. Each carbon atom of the hexagon connected with the Mn atom contributes 0.03 μ_B MM. For the B_1 site, the Mn atom has 5.42 μ_B MM and total MM equals 5.67 μ_B. Each carbon atom connected with the Mn atom has 0.03 μ_B MM. And the nearby carbon atoms have 0.03 μ_B MM. The carbon atoms far away from the adsorption site contribute quite small that can even be neglected. For all considered configurations, the spin density mainly localizes at the adsorption sites and quickly decreases when far away from the adsorption sites. And this point is similar to other TM atoms (Figures 2, 4, and 6).

Among the H_1, H_2, H_3, and B_1 sites, the most stable adsorption site is H_3. Therefore, when two Mn atoms adsorb

Table 3. Adsorption Energies and Structural Properties of the Mn Atom for H_1, H_2, H_3, and B_1 Sites Investigated in This Work[a]

			distance (Å)						
Mn site	E_{tot} (eV)	E_{ad} (eV)	d_1	d_2	d_3	d_4	$\Delta\rho$ (e)	MM (μ_B)	MM_{Mn} (μ_B)
H_2	−684.52	1.16	2.44	2.44	2.44	2.44	0.31	5.23	5.05
H_3	−684.75	1.39	2.30	2.30	2.30	2.30	0.25	5.04	5.06
H_1	−684.28	0.92	2.63	2.63	2.63	2.63	0.29	5.79	5.47
B_1	−683.55	0.19	2.40	2.40			0.26	5.67	5.42

[a]The properties listed are E_{ad} (eV), d_1, d_2, d_3, d_4 (Å), $\Delta\rho$ (e), MM (μ_B), and MM_{Mn} (μ_B).

https://dx.doi.org/10.1021/acsomega.9b04154
ACS Omega 2020, 5, 5900−5910

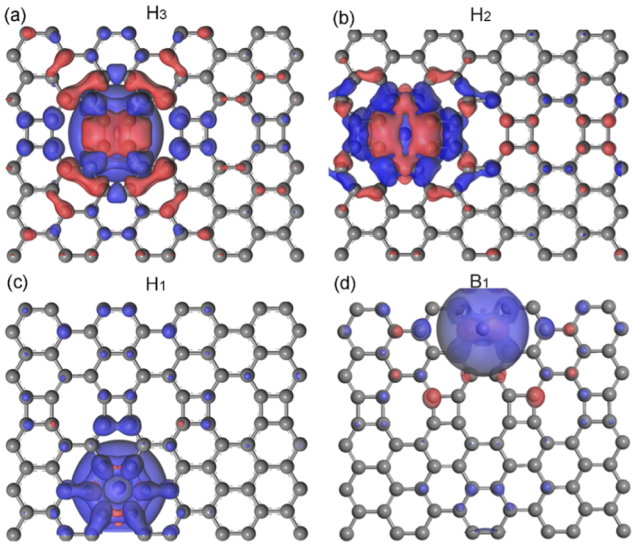

Figure 6. Spin density of Mn atom adsorption on graphene and the corresponding sites of (a) H_3, (b) H_2, (c) H_1, and (d) B_1. And the corresponding isovalue is set to 0.003 e/Å^3.

on graphene, two Mn atoms tend to form a metal line, as shown in Figure 7a,b, respectively. The corresponding Mn−C

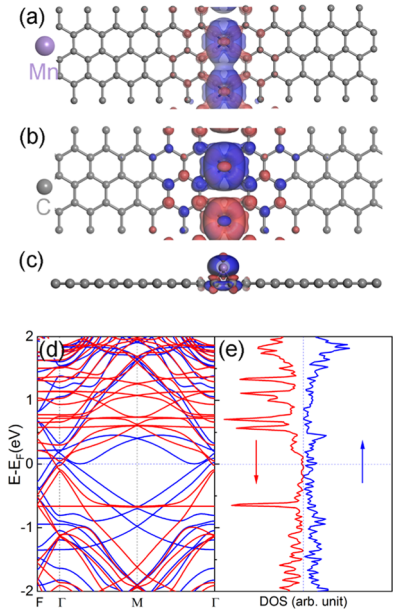

Figure 7. (a) Spin density of (c) FM and (b) AFM configurations of Mn-LD. The red and blue lines represent the spin α and β electrons, respectively. (d) Spin-polarized band structure and (e) DOS of Mn-LD. The medium slate blue and gray balls represent manganese and carbon atoms, respectively.

bond length is 2.31 (2.31 Å × 4) and 2.30 Å (2.30 Å × 4). Two kinds of magnetic configuration FM and AFM are considered. And the corresponding spin density is shown in Figure 7a,b, respectively. ΔE = 0.02 eV. For FM configuration, each Mn atom loses 0.24 e electron, which transfers to graphene. Each Mn atom has 5.00 μ_B MM, and the carbon atoms (eight atoms) of square bonded to the Mn atom contribute −0.01 μ_B MM (−0.01 × 8 μ_B). And the whole system has 10.00 μ_B MM.

For AFM configuration, each Mn atom loses 0.19 e electron. And one Mn atom has 5.00 μ_B MM, while the other has −5.00 μ_B MM. The carbon atoms of the square to the Mn atom (5.00 μ_B MM) has −0.02 μ_B MM, while carbon atoms connected with the Mn atom (−5.00 μ_B MM) have −0.02 μ_B MM, as shown in Figure 7a. The whole system only has 0.00 μ_B, as shown in Figure 7b. The corresponding E_{ad} value is 2.50 eV, which is consistent with the single Mn atom adsorbing on the graphene. The electronic property of Mn-LD at the FM ground state is also calculated, as shown in Figure 7c,d. From the band structures, we can find that both spin-α and spin-β electrons show contribution at the Fermi level. As a result, both spin-α and spin-β electrons could come through the Mn-LDs. By the analysis of the PDOS, we can also find that the states near the Fermi level mainly come from the contribution of Mn atoms. Two peaks at 0.56 and −0.65 eV also come from the contribution of Mn atoms. Besides, there are several Dirac cones existing in the Mn-LD. There is a Dirac cone at 0.19 eV above the Fermi level for the spin-β electrons. There is also a Dirac cone at 0.56 eV above the Fermi level for the spin-β electrons. While for the spin-α electrons, there are two Dirac cones at 0.05 eV above the Fermi level.

3.2.4. Electronic Structure and Magnetic Properties of Ni Atom Adsorption on Graphene. In this part, the structural, magnetic, and electronic properties of the Ni atom adsorption on graphene are systematically investigated. Different adsorption H_2, H_3, H_1, and B_1 sites are investigated, and the results are shown in Table 4. The most stable adsorption site is also the H_3 site, with E_{ad} = 2.28 eV, and the corresponding Ni−C bond length is 2.03 Å (2.03 Å × 4), which is smaller than the Ni−C bond lengths of the H_1 and H_2 sites. The Ni atom loses 0.27 e electron. While for the H_2 site, the corresponding E_{ad} value is 1.58 eV, which means that the B_1 site is the most unstable site in the considering sites. The corresponding Ni−C bond length is 2.14 Å (2.14 Å × 4). And 0.20 e electron is transferred from the Ni atom to the graphene layer. For the H_1 site, the corresponding E_{ad} value is 1.90 eV and the corresponding Ni−C bond lengths is 2.13 Å (2.13 Å × 3) and 2.12 Å (2.12 Å × 3). The graphene gets 0.19 e electron from the Ni atom. For the B_1 site, the corresponding E_{ad} value is 1.72 eV, which is smaller than that of the H_1 and H_3 sites. The corresponding Ni−C bond length is 1.94 Å (1.94 Å × 2), which is the smallest value in the results presented in Table 4. And graphene gets 0.21 e electron from Ni atom. For all of the considered H_1, H_2, H_3, and B_1 sites, both Ni and total MM equal 0.00 μ_B, which is consistent with single Ni atom adsorption on the perfect graphene sheet.[49] Compared to the H_1 (0.19 e), H_2 (0.20 e), and B_1 (0.21 e) sites, the H_3 site has the largest E_{ad}, which corresponds to the largest charge transfer (0.27 e).

For all kinds of adsorption sites, the H_3 site has the largest E_{ad}. So, the two Ni atoms intend to form a line, when the two Ni atoms adsorb on the graphene. In this part, the structural, magnetic, and electronic properties of Ni-LD are calculated. The corresponding Ni−C bond length is 2.04 Å. Each Ni atom loses about 0.18 e electron, and graphene sheet gets 0.36 e electron from two Ni atoms. Each Ni atom has 0.30 μ_B MM, and Ni-LD has 1.00 μ_B MM. The spin density is shown in Figure 8a. The spin density of carbon atoms mainly localizes at the defective zones, and it quickly decays when far away from defective areas. The Ni-LDs are at the FM ground state, and the AFM state is unstable. The E_{ad} value of two Ni atoms adsorption at the H_3 site is 4.30 eV, which is consistent with

https://dx.doi.org/10.1021/acsomega.9b04154
ACS Omega 2020, 5, 5900−5910

Table 4. Adsorption Energies and Structural Properties of Ni Atom for the H_1, H_2, H_3 and B_1 Sites Investigated in This Project[a]

			distance (Å)						
Ni sites	E_{tot} (eV)	E_{ad} (eV)	d_1	d_2	d_3	d_4	$\Delta\rho$ (e)	MM (μ_B)	MM_{Ni} (μ_B)
H_2	−686.42	1.58	2.14	2.14	2.14	2.14	0.20	0	0
H_3	−687.12	2.28	2.03	2.03	2.03	2.03	0.27	0	0
H_1	−686.74	1.90	2.13	2.13	2.12	2.12	0.19	0	0
B_1	−686.56	1.72	1.94	1.94			0.21	0	0

[a]The properties listed are E_{ad} (eV); bond lengths d_1, d_2, d_3, and d_4 (Å); charge transfer between TM and graphene $\Delta\rho$ (e); and total magnetic moments MM (μ_B) and Mn MM_{Ni} (μ_B).

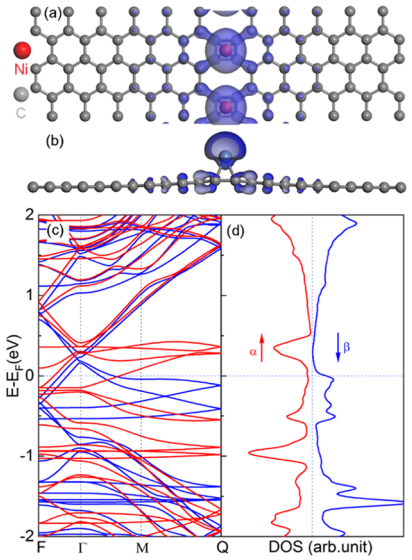

Figure 8. (a–d) DOS and band structures of Ni-LD. The blue and gray balls denote Ni and carbon atoms, respectively. (a–c) Spin-polarized spin density, band structures, and PDOS of Ni-LD, respectively. Top-view (a) and side-view (b) spin density of FM of Ni-LD, (c) band structure, and (d) DOS of Ni-LD. The blue and red lines represent the spin-α and spin-β electrons, respectively. Here, the isovalue is set to 0.003 e/Å^3.

the E_{ad} value of isolated Ni atom adsorption on graphene. The spin-polarized band structure and density of state are also investigated, as shown in Figure 8.

From the band structure, it can be found that Ni-LD is a common spin-polarized metal, and both spin-α and spin-β electrons could make contribution to the conduction. The analysis of DOS is also confirmed by the above analysis. Both spin-α and spin-β electrons have occupied states at the Fermi level, as shown in Figure 8c. Besides, the states near the Fermi level mainly come from the contribution of the Ni and defective carbon atoms. And more details could be found in Figure S4 in the Supporting Information. It is also quite interesting that for the single Ni atom adsorption on graphene, the whole system shows spin-unpolarized ground state. The whole system has no magnetic moment, no matter the Ni atom locates at the H_1, H_2, H_3, or B_1 site. The spin polarization results from the two Ni atoms that ferromagnetically couple with each other. The strain could effectively tune the magnetic and electronic properties of the Ni-LDs.

3.2.5. Electronic Structure and Magnetic Properties of V Atom Adsorption on Graphene. In the above section, the structural, magnetic, and electronic properties of Co, Fe, Mn, and Ni atoms are calculated. In the last part, the structural, magnetic, and electronic properties of V adsorption on the graphene are also calculated, as shown in Table 5. The E_{ad} value of the H_2 site is 2.18 eV, the corresponding V−C bond length is 2.21 Å (2.21 Å × 4), and there is 0.41 e electron transfer from the V atom to the graphene. For the H_3 site, the corresponding E_{ad} value is −2.52 eV, which is obviously bigger than other sites. The corresponding V−C bond length is 2.15 Å (2.15 Å × 4), which is smaller than other configurations. While for the H_1 site, the corresponding V−C bond length is 2.31 Å (2.31 Å × 3) and 2.32 Å (2.32 Å × 3), and the corresponding E_{ad} is 1.82 eV, which is consistent with perfect graphene.[49] For the B_2 site, the V−C bond length is 2.17 Å (2.17 Å × 2) and 2.16 Å (2.16 Å × 2), and the corresponding adsorption energy is 1.75 eV, which are the smallest values in the considering sites, implying that this site is less stable than other sites.

There is an obvious charge transfer between the V atom and graphene. For the H_3 site, the corresponding largest E_{ad} has the highest charge transfer 0.48 e electron. The V atom has 2.96 μ_B MM, and the whole system has 2.69 μ_B MM. For the H_2 site, 0.41 e electron is transferred from the V atom to graphene. And the V atom has 2.59 μ_B MM, while the whole system has 2.84 μ_B MM. Carbon atoms of the square have 0.03 and 0.01 μ_B MM, as shown in Figure 9d. While for the H_1 site, there is 0.41 e electron transfer between the V atom and graphene. And the corresponding V atom has 3.28 μ_B MM, and V-LD has 3.87 μ_B MM, which is consistent with previous results.[49] Each carbon atom connected with the V atom has 0.03 μ_B MM, as

Table 5. Adsorption Energies and Structural Properties of V Atom for H_1, H_2, H_3, and B_1 Sites Investigated in This Work[a]

			distance (Å)						
V sites	E_{tot} (eV)	E_{ad} (eV)	d_1	d_2	d_3	d_4	$\Delta\rho$ (e)	MM (μ_B)	MM_V (μ_B)
H_2	−687.05	2.18	2.21	2.21	2.21	2.21	0.41	2.84	2.59
H_3	−687.39	2.52	2.15	2.15	2.15	2.15	0.48	2.69	2.86
H_1	−686.69	1.82	2.31	2.31	2.32	2.32	0.43	3.87	3.28
B_2	−686.62	1.75	2.16	2.16	2.17	2.17	0.38	2.97	2.99

[a]The properties listed are E_{ad} (eV); bond lengths d_1, d_2, d_3, and d_4 (Å); charge transfer between TM and graphene $\Delta\rho$ (e); and total magnetic moments MM (μ_B) and V MM_V (μ_B).

https://dx.doi.org/10.1021/acsomega.9b04154
ACS Omega 2020, 5, 5900−5910

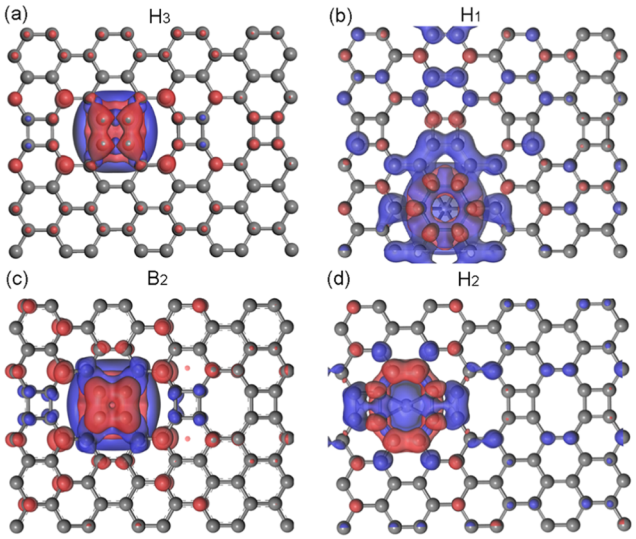

Figure 9. Spin density of single V atom adsorption on graphene with LD. (a–d) Different adsorption sites: (a) H_3, (b) H_1, (c) B_2, and (d) H_2. The isovalue is set to 0.003 e/Å^3.

shown in Figure 9b. For the B_1 site, V loses 0.38 e electron. The V atom has 2.99 μ_B MM. More details are found in Figure 9c.

As discussed above, the magnetic moment also mainly localizes at adsorption sites. The V atom prefers to stay at the H_3 site, and two V atoms intend to form an "extended metallic wire". The structural, magnetic, and electronic properties of the "metallic wire" are still unknown. In the following part, the geometry and the magnetic and electronic properties are investigated. Based on the coupling of two V atoms, there are two kinds of magnetic configuration. The FM and AFM configurations are calculated as shown in Figure 10a,b, respectively. So, ΔE = 0.12 eV, which implies its FM ground state. For the AFM configuration, one V atom has 2.89 μ_B MM, while the other V atom has −2.89 μ_B MM. For lower energy of FM configuration, both V atoms have 2.89 μ_B MM. The corresponding E_{ad} value is 4.96 eV, which is consistent with the H_3 site. The spin-polarized band structure and density of state at the FM state are also calculated, as shown in Figure 10c,d, respectively. The spin-α electron is conductive, while the spin-β electron is an insulator with a band gap of 0.20 eV. Therefore, V-LD is a half-metal. Besides, there is a Dirac cone composed of spin-α electrons, whose position can be modulated by strains. The half-metallicity is confirmed by the analysis of the density of states, and the states near the Fermi level mainly come from the contribution of the V atom and defective carbon atoms.

3.3. Biaxial Strains Tune the Electronic Structure Properties of TM-LD. When the nanodevices work, they have to be constructed and measured on certain substrates. There is lattice mismatch between all kinds of materials. To simplify these issues, we use the strain to simulate this situation and the stability of the half-metallicity under the strains is also investigated. Only the enlarged strain along lattice $\vec{a}$ is investigated, and spin-polarized band structures under strains of 1 and 2% are also calculated, as shown in Figure S5. Though the band gap of the spin-β electron is decreased (0.07 eV for 1%, 0.04 eV for 2%), Co-LD still shows half-metallicity. More details and discussion are provided in the Supporting Information.

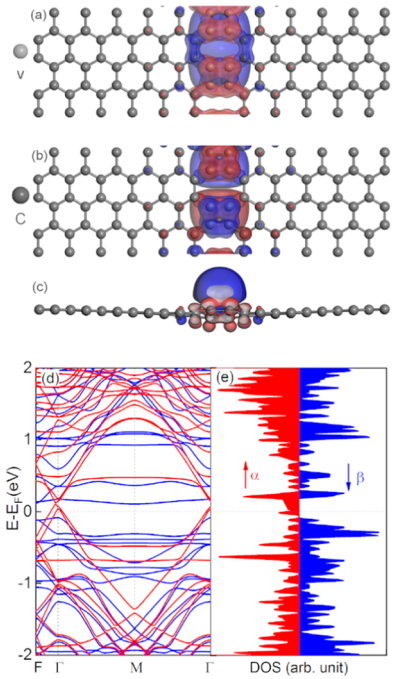

Figure 10. (a–e) Spin density, spin-polarized band structure, and PDOS of V-LD. (a) Spin density of (c) FM and (b) AFM configurations of V-LD. (d) Band structure and (e) DOS of V-LD at the FM ground state. The blue and red lines represent spin-α and β electrons, respectively. Gray and black denote vanadium and carbon atoms, respectively. Here, the isovalue is set to 0.003 e/Å^3.

The strain is also generally used as an effective method to modulate the electronic properties of low-dimensional materials.[19] So, the effect of strain on the magnetic and electronic properties of Fe-LD is also investigated. We systematically investigate the effect of the enlarged strains. The spin-polarized band structures of Fe-LDs under +2 and +4% strains along the $\vec{a}$ direction are calculated, as shown in Figure S6a,b, respectively. With an enlarged strain of +2%, Fe-LD still presents half-metallic properties. And there is a Dirac cone lying 0.04 eV above the Fermi level for spin-α electrons, while it presents semiconductor with a band gap of 0.14 eV for spin-β electrons. As the strain is enlarged to +4%, Fe-LD presents semimetal with Dirac cone for spin-α electrons, while it shows semiconductive properties for spin-β electrons with a band gap of 0.13 eV, as shown in Figure S6b. So, smaller enlarged strains could effectively tune Fe-LD spin-polarized metal into a half-metal and even degenerate original Dirac cones composed of spin-α and spin-β electrons.

As discussed above, the strains could effectively tune the position of Dirac cone. So, the band structures of Mn-LDs under the enlarged strain are also investigated, as shown in Figure S7 in the Supporting information. We mainly considered the enlarged strains of +1, +2, +3, and +4%. And the corresponding band structures are shown in Figure S7a–d. A Dirac cone of spin-α electron is shifted from the original 0.05 eV above the Fermi level to −0.01 eV below the Fermi level under 1% enlarged strain. As the enlarged strain is increased to 2%, two Dirac cones for spin-α electron are continuously shifted −0.015 eV below the Fermi level. While other Dirac cones composed of spin-α and spin-β electrons are shifted 0.05 eV above the Fermi level. As the enlarged strain is increased to 3%, two Dirac cones composed of spin-α electron are shifted downward −0.02 eV below the Fermi level. And

https://dx.doi.org/10.1021/acsomega.9b04154
ACS Omega 2020, 5, 5900−5910

there is a special Dirac cone composed of spin-α and spin-β electrons lying 0.01 eV above the Fermi level. As the enlarged strain is increased to 4%, two Dirac cones composed of spin-α electrons are shifted down −0.03 eV below the Fermi level. In a word, the position of Dirac cone can be tuned by the enlarged strains, which means that Mn-LD could be applied in valley and spin electronics.

The stability of V-LD under the enlarged strains along $\vec{a}$ is also investigated, shown in Figure S8. We can find that V-LD is still at the FM ground state and still shows half-metallicity. As the strain increases, the position of Dirac cone is tuned by strains. And the band gap of spin-α electrons monotonously decreases with increase of strains. For smaller strains (less than 3%), V-LD still shows half-metallic properties. As the strain is increased to 4%, the band edge of spin-α electron is shifted upward, even across the Fermi level. And V-LD changes from half-metal to normal spin-polarized metal. Therefore, the stability of half-metallicity of V-LD is well preserved, when the enlarged strain is less than 3%.

4. CONCLUSIONS

In conclusion, we examine the geometry and the magnetic and electronic properties of TM adsorption on graphene with LD. For Co, Fe, Mn, Ni, and V atoms, the most stable configuration is the H_2 site, which has the largest E_{ad} value. When a single TM (TM = Co, Fe, Mn, V) atom adsorbs on graphene, it introduces localized magnetism around TM and carbon atoms near the TM atom. And the corresponding magnetism mainly comes from the contribution of TM atoms. When two TM atoms adsorb on graphene, they tend to stay at the H_2 site, forming a metallic line, which can work as a conductive metallic wire. All of the above-mentioned metal adsorption on graphene can introduce magnetism and spin polarization, and they are all at the FM ground state, while different metals show different electronic properties. TM-LD (TM = Co, V) is a spin-polarized half-metal, while TM-LD (TM = Fe, Mn, Ni) is a spin-polarized metal at the FM ground state. And uniaxial strains along the $\vec{a}$ direction could tune TM-LD into half-metal (TM = Fe, Co, V) or semimetal (TM = Mn) with Dirac cones (composed of one or two kinds of electrons spin). These theoretical findings could open the door to the application in spintronics[9,62] and valley electrons.[24,61] This opens up the exciting possibility of the fabrication of carbon-based electronic devices with one-dimensional extended LDs that can be used as metallic wire interconnects or elements of device structures.

■ ASSOCIATED CONTENT

Supporting Information

The Supporting Information is available free of charge at https://pubs.acs.org/doi/10.1021/acsomega.9b04154.

Information on materials, magnetic moment distribution, PDOS of Co-LD, band structure of Co-LDs under the enlarged strains, PDOS of Fe-LDs, band structures of Mn-LDs under strains, band structures of V-LDs under enlarged strains, and band structures of V-LDs under enlarged strain (PDF)

■ AUTHOR INFORMATION

Corresponding Author

Zhaoyong Guan − *School of Chemistry and Chemical Engineering, Shandong University, Jinan 250100, P. R. China; Department of Physics, Tsinghua University, Beijing 100084, P. R. China;* orcid.org/0000-0002-5304-028X; Phone: +86-0531-88361168; Email: zyguan@sdu.edu.cn; Fax: +86-88361168

Authors

Shuang Ni − *Research Center of Laser Fusion, China Academy of Engineering Physics, Mianyang, Sichuan 621900, P. R. China*

Shuanglin Hu − *Institute of Nuclear Physics and Chemistry, China Academy of Engineering Physics, Mianyang, Sichuan 621900, P. R. China*

Complete contact information is available at: https://pubs.acs.org/10.1021/acsomega.9b04154

Notes

The authors declare no competing financial interest.

■ ACKNOWLEDGMENTS

The authors thank Dr. Xingxing Li, Haifeng Lv, and Professor Wenhui Duan for useful discussion. This project was partially funded by the President Foundation of China Academy of Engineering Physics (YZJJLX2016004), the National Key Research and Development Program of China (Grant No. 2016YFB0201203), National Natural Science Foundation of China (Grant No. 11904203), and the Fundamental Research Funds of Shandong University (Grant No. 2019GN065). The Shanghai Supercomputer Center, National Supercomputing Centers of Guangzhou, and Supercomputer Centers of Tsinghua University are also acknowledged.

■ REFERENCES

(1) Novoselov, K. S.; Geim, A. K.; Morozov, S. V.; Jiang, D.; Zhang, Y.; Dubonos, S. V.; Grigorieva, I. V.; Firsov, A. A. Electric Field Effect in Atomically Thin Carbon Films. *Science* **2004**, *306*, 666−669.

(2) Wallace, P. R. The Band Theory of Graphite. *Phys. Rev.* **1947**, *71*, 622−634.

(3) Katsnelson, M. I.; Novoselov, K. S.; Geim, A. K. Chiral Tunnelling and the Klein Paradox In graphene. *Nat. Phys.* **2006**, *2*, 620−625.

(4) Neto, A. C.; Guinea, F.; Peres, N. M. Drawing Conclusions from Graphene. *Phys. World* **2006**, *19*, 33−37.

(5) Katsnelson, M. I.; Novoselov, K. S. Graphene: New Bridge between Condensed Matter Physics and Quantum Electrodynamics. *Solid State Commun.* **2007**, *143*, 3−13.

(6) Castro Neto, A. H.; Guinea, F.; Peres, N. M. R.; Novoselov, K. S.; Geim, A. K. The Electronic Properties of Graphene. *Rev. Mod. Phys.* **2009**, *81*, 109.

(7) Du, X.; Skachko, I.; Barker, A.; Andrei, E. Y. Approaching Ballistic Transport in Suspended Graphene. *Nat. Nanotechnol.* **2008**, *3*, 491.

(8) Castro, E. V.; Ochoa, H.; Katsnelson, M. I.; Gorbachev, R. V.; Elias, D. C.; Novoselov, K. S.; Geim, A. K.; Guinea, F. Limits on Charge Carrier Mobility in Suspended Graphene Due to Flexural Phonons. *Phys. Rev. Lett.* **2010**, *105*, No. 266601.

(9) Son, Y.-W.; Cohen, M. L.; Louie, S. G. Half-Metallic Graphene Nanoribbons. *Nature* **2006**, *444*, 347.

(10) Kan, E.-J.; Li, Z.; Yang, J.; Hou, J. G. Will Zigzag Graphene Nanoribbon Turn to Half Metal under Electric Field? *Appl. Phys. Lett.* **2007**, *91*, No. 243116.

(11) Guan, Z.; Ni, S.; Hu, S. Tuning the Electronic and Magnetic Properties of Graphene Flake Embedded in Boron Nitride Nanoribbons with Transverse Electric Fields: First-Principles Calculations. *ACS Omega* **2019**, *4*, 10293−10301.

(12) Guan, Z.; Wang, J.; Huang, J.; Wu, X.; Li, Q.; Yang, J. Metal-Free Magnetism and Half-Metallicity of Carbon Nitride Nanotubes: A First-Principles Study. *J. Phys. Chem. C* **2014**, *118*, 22491−22498.

(13) Guan, Z.; Wang, W.; Huang, J.; Wu, X.; Li, Q.; Yang, J. Tunable Electronic and Magnetic Properties of Graphene Flake-Doped Boron Nitride Nanotubes. *J. Phys. Chem. C* **2014**, *118*, 28616−28624.
(14) Guan, Z.; Si, C.; Hu, S.; Duan, W. First-Principles Study of Line-Defect-Embedded Zigzag Graphene Nanoribbons: Electronic and Magnetic Properties. *Phys. Chem. Chem. Phys.* **2016**, *18*, 12350−12356.
(15) Kan, E.-J.; Li, Z.; Yang, J.; Hou, J. G. Half-Metallicity in Edge-Modified Zigzag Graphene Nanoribbons. *J. Am. Chem. Soc.* **2008**, *130*, 4224−4225.
(16) Liu, H.; Liu, Y.; Zhu, D. Chemical Doping of Graphene. *J. Mater. Chem.* **2011**, *21*, 3335−3345.
(17) Ci, L.; Song, L.; Jin, C.; Jariwala, D.; Wu, D.; Li, Y.; Srivastava, A.; Wang, Z. F.; Storr, K.; Balicas, L.; Liu, F.; Ajayan, P. M. Atomic Layers of Hybridized Boron Nitride and Graphene Domains. *Nat. Mater.* **2010**, *9*, 430.
(18) Fan, X.; Shen, Z.; Liu, A. Q.; Kuo, J.-L. Band Gap Opening of Graphene by Doping Small Boron Nitride Domains. *Nanoscale* **2012**, *4*, 2157−2165.
(19) Guan, Z.; Ni, S.; Hu, S. Band Gap Opening of Graphene by Forming a Graphene/$PtSe_2$ Van Der Waals Heterojunction. *RSC Adv.* **2017**, *7*, 45393−45399.
(20) Guan, Z.; Ni, S.; Hu, S. Tunable Electronic and Optical Properties of Monolayer and Multilayer Janus Mosse as a Photocatalyst for Solar Water Splitting: A First-Principles Study. *J. Phys. Chem. C* **2018**, *122*, 6209−6216.
(21) Guan, Z.; Lian, C.-S.; Hu, S.; Ni, S.; Li, J.; Duan, W. Tunable Structural, Electronic, and Optical Properties of Layered Two-Dimensional C_2N and MoS_2 Van Der Waals Heterostructure as Photovoltaic Material. *J. Phys. Chem. C* **2017**, *121*, 3654−3660.
(22) Lin, X.; Ni, J. Half-Metallicity in Graphene Nanoribbons with Topological Line Defects. *Phys. Rev. B* **2011**, *84*, No. 075461.
(23) Dai, Q. Q.; Zhu, Y. F.; Jiang, Q. Electronic and Magnetic Engineering in Zigzag Graphene Nanoribbons Having a Topological Line Defect at Different Positions with or without Strain. *J. Phys. Chem. C* **2013**, *117*, 4791−4799.
(24) Gunlycke, D.; White, C. T. Graphene Valley Filter Using a Line Defect. *Phys. Rev. Lett.* **2011**, *106*, No. 136806.
(25) Mananghaya, M. R. Titanium-Decorated Boron Nitride Nanotubes for Hydrogen Storage: A Multiscale Theoretical Investigation. *Nanoscale* **2019**, *11*, 16052−16062.
(26) Mananghaya, M. R.; Santos, G. N.; Yu, D. Hydrogen Adsorption of Ti-Decorated Boron Nitride Nanotube: A Density Functional Based Tight Binding Molecular Dynamics Study. *Adsorption* **2018**, *24*, 683−690.
(27) Mananghaya, M. R. A Simulation of Hydrogen Adsorption/Desorption in Metal-Functionalized Bn Nanotube. *Mater. Chem. Phys.* **2020**, *240*, No. 122159.
(28) Boukhvalov, D. W.; Katsnelson, M. I. Chemical Functionalization of Graphene with Defects. *Nano Lett.* **2008**, *8*, 4373−4379.
(29) Zhang, D.; Long, M.; Zhang, X.; Ouyang, F.; Li, M.; Xu, H. Designing of Spin-Filtering Devices in Zigzag Graphene Nanoribbons Heterojunctions by Asymmetric Hydrogenation and B-N Doping. *J. Appl. Phys.* **2015**, *117*, No. 014311.
(30) Yang, X.-F.; Zhou, W.-Q.; Hong, X.-K.; Liu, Y.-S.; Wang, X.-F.; Feng, J.-F. Half-Metallic Properties, Single-Spin Negative Differential Resistance, and Large Single-Spin Seebeck Effects Induced by Chemical Doping in Zigzag-Edged Graphene Nanoribbons. *J. Chem. Phys.* **2015**, *142*, No. 024706.
(31) Yu, G.; Zhu, M.; Zheng, Y. First-Principles Study of 3*d* Transition Metal Atom Adsorption onto Graphene: The Role of the Extended Line Defect. *J. Mater. Chem. C* **2014**, *2*, 9767−9774.
(32) Zhu, Z.; Chen, W.; Sun, Q.; Jia, Y. Half-Metal Behaviour Mediated by Self-Doping of Topological Line Defect Combining with Adsorption of 3*d* Transition-Metal Atomic Chains in Graphene. *J. Phys. D: Appl. Phys.* **2014**, *47*, No. 055303.
(33) Yang, Y.; Xiao, Y.; Ren, W.; Yan, X. H.; Pan, F. Half-Metallic Chromium-Chain-Embedded Wire in Graphene and Carbon Nanotubes. *Phys. Rev. B* **2011**, *84*, No. 195447.
(34) Wang, H.; Wang, Q.; Cheng, Y.; Li, K.; Yao, Y.; Zhang, Q.; Dong, C.; Wang, P.; Schwingenschlögl, U.; Yang, W.; Zhang, X. X. Doping Monolayer Graphene with Single Atom Substitutions. *Nano Lett.* **2012**, *12*, 141−144.
(35) Dai, J.; Yuan, J. Adsorption of Molecular Oxygen on Doped Graphene: Atomic, Electronic, and Magnetic Properties. *Phys. Rev. B* **2010**, *81*, No. 165414.
(36) He, T.; Zhang, C.; Du, A. Single-Atom Supported on Graphene Grain Boundary as an Efficient Electrocatalyst for Hydrogen Evolution Reaction. *Chem. Eng. Sci.* **2019**, *194*, 58−63.
(37) Wang, X.; Wang, J.; Wang, D.; Dou, S.; Ma, Z.; Wu, J.; Tao, L.; Shen, A.; Ouyang, C.; Liu, Q.; Wang, S. One-Pot Synthesis of Nitrogen and Sulfur Co-Doped Graphene as Efficient Metal-Free Electrocatalysts for the Oxygen Reduction Reaction. *Chem. Commun.* **2014**, *50*, 4839−4842.
(38) Niu, F.; Liu, J.-M.; Tao, L.-M.; Wang, W.; Song, W.-G. Nitrogen and Silica Co-Doped Graphene Nanosheets for No2 Gas Sensing. *J. Mater. Chem. A* **2013**, *1*, 6130−6133.
(39) Fei, H.; Dong, J.; Arellano-Jiménez, M. J.; Ye, G.; Dong Kim, N.; Samuel, E. L. G.; Peng, Z.; Zhu, Z.; Qin, F.; Bao, J.; Yacaman, M. J.; Ajayan, P. M.; Chen, D.; Tour, J. M. Atomic Cobalt on Nitrogen-Doped Graphene for Hydrogen Generation. *Nat. Commun.* **2015**, *6*, No. 8668.
(40) Xu, Q.; Yang, G.; Fan, X.; Zheng, W. Improving the Quantum Capacitance of Graphene-Based Supercapacitors by the Doping and Co-Doping: First-Principles Calculations. *ACS Omega* **2019**, *4*, 13209−13217.
(41) Jiang, H.; Yao, Y.; Zhu, Y.; Liu, Y.; Su, Y.; Yang, X.; Li, C. Iron Carbide Nanoparticles Encapsulated in Mesoporous Fe−N-Doped Graphene-Like Carbon Hybrids as Efficient Bifunctional Oxygen Electrocatalysts. *ACS Appl. Mater. Interfaces* **2015**, *7*, 21511−21520.
(42) Robertson, A. W.; Montanari, B.; He, K.; Kim, J.; Allen, C. S.; Wu, Y. A.; Olivier, J.; Neethling, J.; Harrison, N.; Kirkland, A. I.; Warner, J. H. Dynamics of Single Fe Atoms in Graphene Vacancies. *Nano Lett.* **2013**, *13*, 1468−1475.
(43) Lim, D.-H.; Negreira, A. S.; Wilcox, J. DFT Studies on the Interaction of Defective Graphene-Supported Fe and Al Nanoparticles. *J. Phys. Chem. C* **2011**, *115*, 8961−8970.
(44) Wu, M.; Cao, C.; Jiang, J. Z. Electronic Structure of Substitutionally Mn-Doped Graphene. *New J. Phys.* **2010**, *12*, No. 063020.
(45) Lei, T.-M.; Liu, J.-J.; Zhang, Y.-M.; Guo, H.; Zhang, Z.-Y. A Quantum Explanation of the Magnetic Properties of Mn-Doped Graphene. *Chin. Phys. B* **2013**, *22*, No. 117502.
(46) Qiu, H.-J.; Ito, Y.; Cong, W.; Tan, Y.; Liu, P.; Hirata, A.; Fujita, T.; Tang, Z.; Chen, M. Nanoporous Graphene with Single-Atom Nickel Dopants: An Efficient and Stable Catalyst for Electrochemical Hydrogen Production. *Angew. Chem., Int. Ed.* **2015**, *54*, 14031−14035.
(47) Rigo, V. A.; Martins, T. B.; da Silva, A. J. R.; Fazzio, A.; Miwa, R. H. Electronic, Structural, and Transport Properties of Ni-Doped Graphene Nanoribbons. *Phys. Rev. B* **2009**, *79*, No. 075435.
(48) Mahmood, N.; Zhang, C.; Hou, Y. Nickel Sulfide/Nitrogen-Doped Graphene Composites: Phase-Controlled Synthesis and High Performance Anode Materials for Lithium Ion Batteries. *Small* **2013**, *9*, 1321−1328.
(49) Manadé, M.; Viñes, F.; Illas, F. Transition Metal Adatoms on Graphene: A Systematic Density Functional Study. *Carbon* **2015**, *95*, 525−534.
(50) Cao, C.; Wu, M.; Jiang, J.; Cheng, H.-P. Transition Metal Adatom and Dimer Adsorbed on Graphene: Induced Magnetization and Electronic Structures. *Phys. Rev. B* **2010**, *81*, No. 205424.
(51) Mao, Y.; Yuan, J.; Zhong, J. Density Functional Calculation of Transition Metal Adatom Adsorption on Graphene. *J. Phys.: Condens. Matter* **2008**, *20*, No. 115209.
(52) Sevinçli, H.; Topsakal, M.; Durgun, E.; Ciraci, S. Electronic and Magnetic Properties of 3*d* Transition-Metal Atom Adsorbed Graphene and Graphene Nanoribbons. *Phys. Rev. B* **2008**, *77*, No. 195434.

https://dx.doi.org/10.1021/acsomega.9b04154
ACS Omega 2020, 5, 5900−5910

(53) Giovannetti, G.; Khomyakov, P. A.; Brocks, G.; Karpan, V. M.; van den Brink, J.; Kelly, P. J. Doping Graphene with Metal Contacts. *Phys. Rev. Lett.* **2008**, *101*, No. 026803.
(54) Chan, K. T.; Neaton, J. B.; Cohen, M. L. First-Principles Study of Metal Adatom Adsorption on Graphene. *Phys. Rev. B* **2008**, *77*, No. 235430.
(55) Nilius, N.; Wallis, T. M.; Ho, W. Development of One-Dimensional Band Structure in Artificial Gold Chains. *Science* **2002**, *297*, 1853−1856.
(56) Liu, M.; Liu, M.; She, L.; Zha, Z.; Pan, J.; Li, S.; Li, T.; He, Y.; Cai, Z.; Wang, J.; Zheng, Y.; Qiu, X.; Zhong, D. Graphene-Like Nanoribbons Periodically Embedded with Four- and Eight-Membered Rings. *Nat. Commun.* **2017**, *8*, No. 14924.
(57) Guan, Z.; Wu, X.; Li, Q. Electronic, Magnetic, and Mechanical Properties of Line-Defect Embedded Graphene Nanoribbons: A First-Principles Study. *Nano LIFE* **2012**, *02*, No. 1240003.
(58) Feng, X.; Maier, S.; Salmeron, M. Water Splits Epitaxial Graphene and Intercalates. *J. Am. Chem. Soc.* **2012**, *134*, 5662−5668.
(59) Mananghaya, M. R.; Santos, G. N.; Yu, D. Solubility of Aminotriethylene Glycol Functionalized Single Wall Carbon Nanotubes: A Density Functional Based Tight Binding Molecular Dynamics Study. *J. Comput. Chem.* **2019**, *40*, 952−958.
(60) Obodo, J. T.; Kahaly, M. U.; Schwingenschlögl, U. Magnetoresistance of Mn-Decorated Topological Line Defects in Graphene. *Phys. Rev. B* **2015**, *91*, No. 014413.
(61) Rycerz, A.; Tworzydło, J.; Beenakker, C. W. J. Valley Filter and Valley Valve in Graphene. *Nat. Phys.* **2007**, *3*, 172.
(62) Han, W.; Kawakami, R. K.; Gmitra, M.; Fabian, J. Graphene Spintronics. *Nat. Nanotechnol.* **2014**, *9*, 794.
(63) Zhou, S. Y.; Siegel, D. A.; Fedorov, A. V.; Lanzara, A. Metal to Insulator Transition in Epitaxial Graphene Induced by Molecular Doping. *Phys. Rev. Lett.* **2008**, *101*, No. 086402.
(64) Prins, F.; Barreiro, A.; Ruitenberg, J. W.; Seldenthuis, J. S.; Aliaga-Alcalde, N.; Vandersypen, L. M. K.; van der Zant, H. S. J. Room-Temperature Gating of Molecular Junctions Using Few-Layer Graphene Nanogap Electrodes. *Nano Lett.* **2011**, *11*, 4607−4611.
(65) Moon, J. S.; Curtis, D.; Hu, M.; Wong, D.; McGuire, C.; Campbell, P. M.; Jernigan, G.; Tedesco, J. L.; VanMil, B.; Myers-Ward, R.; Eddy, C., Jr.; Gaskill, D. K. Epitaxial-Graphene Rf Field-Effect Transistors on Si-Face 6H-Sic Substrates. *IEEE Electron Device Lett.* **2009**, *30*, 650−652.
(66) Sethulakshmi, N.; Mishra, A.; Ajayan, P. M.; Kawazoe, Y.; Roy, A. K.; Singh, A. K.; Tiwary, C. S. Magnetism in Two-Dimensional Materials Beyond Graphene. *Mater. Today* **2019**, *27*, 107−122.
(67) Stolyarova, E.; Stolyarov, D.; Bolotin, K.; Ryu, S.; Liu, L.; Rim, K. T.; Klima, M.; Hybertsen, M.; Pogorelsky, I.; Pavlishin, I.; Kusche, K.; Hone, J.; Kim, P.; Stormer, H. L.; Yakimenko, V.; Flynn, G. Observation of Graphene Bubbles and Effective Mass Transport under Graphene Films. *Nano Lett.* **2009**, *9*, 332−337.
(68) Bunch, J. S.; Verbridge, S. S.; Alden, J. S.; van der Zande, A. M.; Parpia, J. M.; Craighead, H. G.; McEuen, P. L. Impermeable Atomic Membranes from Graphene Sheets. *Nano Lett.* **2008**, *8*, 2458−2462.
(69) Schedin, F.; Geim, A. K.; Morozov, S. V.; Hill, E. W.; Blake, P.; Katsnelson, M. I.; Novoselov, K. S. Detection of Individual Gas Molecules Adsorbed on Graphene. *Nat. Mater.* **2007**, *6*, 652−655.
(70) Jia, Y.; Jiang, K.; Wang, H.; Yao, X. The Role of Defect Sites in Nanomaterials for Electrocatalytic Energy Conversion. *Chem* **2019**, *5*, 1371−1397.
(71) Delley, B. An All-Electron Numerical Method for Solving the Local Density Functional for Polyatomic Molecules. *J. Chem. Phys.* **1990**, *92*, 508−517.
(72) Delley, B. From Molecules to Solids with the Dmol(3) Approach. *J. Chem. Phys.* **2000**, *113*, 7756−7764.
(73) Perdew, J. P.; Burke, K.; Ernzerhof, M. Generalized Gradient Approximation Made Simple. *Phys. Rev. Lett.* **1996**, *77*, 3865−3868.
(74) Delley, B. The Conductor-Like Screening Model for Polymers and Surfaces. *Mol. Simul.* **2006**, *32*, 117−123.
(75) Monkhorst, H. J.; Pack, J. D. Special Points for Brillouin-Zone Integrations. *Phys. Rev. B* **1976**, *13*, 5188−5192.
(76) Hirshfeld, F. L. Bonded-Atom Fragments for Describing Molecular Charge Densities. *Theor. Chim. Acta* **1977**, *44*, 129−138.
(77) Jiang, C.-H.; Chen, Q.; Ge, G.-X.; Li, Y.-B.; Wan, J.-G. Structure and Spin-Polarized Transport of Co Atomic Chains on Graphene with Topological Line Defects. *J. Cluster Sci.* **2016**, *27*, 875−882.
(78) Lahiri, J.; Lin, Y.; Bozkurt, P.; Oleynik, I. I.; Batzill, M. An Extended Defect in Graphene as a Metallic Wire. *Nat. Nanotechnol.* **2010**, *5*, 326.

https://dx.doi.org/10.1021/acsomega.9b04154
ACS Omega 2020, 5, 5900−5910